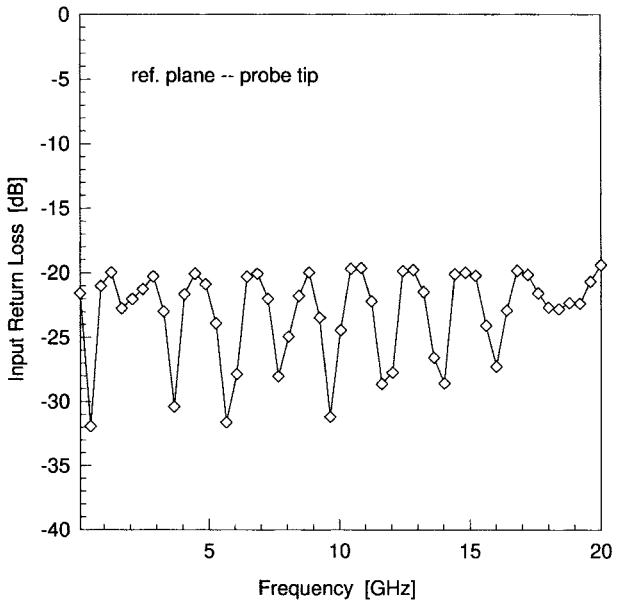

Fig. 5. Measured input return loss of the device.

accurate measurements when the contacts pads are partially or fully suspended.

The input mismatch measurements in Fig. 5 show acceptable mismatch error below -20 dB at all frequencies. As a result of the mismatch, the frequency dependence measurements from Fig. 4 have some further uncertainty, but can be neglected because of the small reflection coefficients. Also, as mentioned earlier, the s_{11} measurements were performed with probe tip calibration, including the parasitics in the probing pads and the underlying silicon. It is expected that the actual input return loss of the device without the pads would be even lower.

V. Conclusions

We presented a novel method for fabricating efficient microwave power sensors in CMOS technology, with an additional low-cost post-process step. The sensors are based on thermocouple measurement techniques. The devices show excellent linearity characteristics, and low return loss up to 20 GHz. The CMOS implementation gives the advantages of low cost and easy integration with CMOS circuits. The future goal is to integrate the devices with sensing and data conversion circuits on the same chip.

Acknowledgment

The authors wish to extend their thanks to RF Microsystems' Senior Scientist E. Bowen for technical discussions and reading of the manuscript. They would also like to acknowledge N. Tea and D. Berning for helpful discussions.

References

[1] D. Jaeggi and H. Baltes, "Thermoelectric AC power sensor by CMOS technology," *IEEE Electron Device Lett.*, vol. 13, pp. 366–368, July 1992.

[2] M. E. Goff and C. A. Barratt, "DC to 40 GHz MMIC power sensor," in *12th Annu. GaAs IC Symp. Tech. Dig.*, New Orleans, LA, Oct. 1990, pp. 105–108.

[3] L. A. Christel and K. Petersen, "A miniature microwave detector using advanced micromachining," in *IEEE Solid-State Sensors Actuator Workshop Tech. Dig.*, Hilton Head, SC, June 1992, pp. 144–147.

[4] P. Kopystynski, E. Obermeier, H. Delfs, and A. Loeser, "Silicon power microsensor with frequency range from DC to microwave," in *Int. Conf. Solid-State Sensors Actuators Dig.*, June 1991, pp. 623–626.

[5] V. Milanović, M. Gaitan, E. D. Bowen, and M. E. Zaghloul, "Micromachined microwave transmission lines in CMOS technology," *IEEE Trans. Microwave Theory Tech.*, vol. 45, pp. 630–635, May 1997.

[6] J. Y.-C. Chang, A. A. Abidi, and M. Gaitan, "Large suspended inductors on silicon and their use in a 2-μm CMOS RF amplifier," *IEEE Electron Device Lett.*, vol. 14, pp. 246–248, May 1993.

[7] L. P. B. Katehi, G. M. Rebeiz, T. M. Weller, R. F. Drayton, H. Cheng, and J. F. Whitaker, "Micromachined circuits for millimeter- and submillimeter-wave applications," *IEEE Antennas Propagat. Mag.*, vol. 35, pp. 9–17, Oct. 1993.

[8] M. Gaitan, J. R. Kinard, and D. X. Huang, "Performance of commercial CMOS foundry-compatible multijunction thermal converters," in *Proc. 7th Int. Conf. Solid-State Sensors Actuators*, Yokohama, Japan, June 1993, pp. 1012–1014.

[9] N. H. Tea, V. Milanović, C. A. Zincke, J. S. Suehle, M. Gaitan, M. E. Zaghloul, and J. Geist, "Hybrid post-processing etching for CMOS-compatible MEMS," *J. Microelectromech. Syst.*, vol. 6, pp. 363–372, Dec. 1997.

[10] R. B. Marks, "A multiline method of network analyzer calibration," *IEEE Trans. Microwave Theory Tech.*, vol. 39, pp. 1205–1215, July 1991.

Simple and Efficient Computation of Electromagnetic Fields in Arbitrarily Shaped Inhomogeneous Dielectric Bodies Using Transpose-Free QMR and FFT

C. F. Wang and J. M. Jin

***Abstract*— A simple and efficient numerical method is presented for computing electromagnetic fields in three-dimensional (3-D) inhomogeneous dielectric bodies. The method employs a two-stage discretization to convert an integro–differential equation into an implicit system of linear algebraic equations. This discrete system is then solved using a transpose-free quasi-minimal residual (TFQMR) algorithm, which avoids the calculation of the multiplication between the transpose of the system matrix and a vector. The simple multiplication between the system matrix and a vector required in the TFQMR algorithm is calculated efficiently using only six fast Fourier transforms (FFT's). Numerical results for strongly inhomogenous and lossy spheres show that the method has a stable convergence behavior and excellent numerical performance.**

***Index Terms*—Electromagnetic field, fast Fourier transform, inhomogeneous dielectric bodies, transpose-free quasi-minimal residual algorithm.**

I. Introduction

Efficient computation of electromagnetic fields in arbitrarily shaped inhomogeneous dielectric bodies in a three-dimensional (3-D) space

Manuscript received January 13, 1997; revised December 5, 1997. This work was supported by the Office of Naval Research under Grant N00014-95-1-0848, by the National Science Foundation under Grant NSF ECE 94-57735, and by a grant from the Air Force Office of Scientific Research via the MURI program under Contract F49620-96-1-0025.

The authors are with the Center for Computational Electromagnetics, Department of Electrical and Computer Engineering, University of Illinois at Urbana-Champaign, Urbana, IL 61801-2991 USA.

Publisher Item Identifier S 0018-9480(98)03169-X.

plays an important role in many applications such as nondestructive testing, microwave imaging, scattering control, target identification, electromagnetic hyperthermia, and magnetic resonance imaging. The well-known method of moments (MoM) [1]–[3] is one of the popular methods for this computation. In this method, an integro–differential equation is first formulated in terms of a volumetric equivalent current that accounts for the effect of the permittivity and conductivity of an inhomogeneous body. This integro–differential equation is then discretized using mostly Galerkin's procedure. The discretization results in a matrix equation with a very large number of unknowns, whose solution using a direct solver, such as Gaussian elimination and an LU decomposition method, is basically impractical because a direct solver has a memory requirement of $O(N^2)$ and computational complexity of $O(N^3)$, where N denotes the number of unknowns. This difficulty can be circumvented by solving the matrix equation using an iterative solver, and in each iteration the required matrix–vector multiplication is evaluated using the fast Fourier transform (FFT) [4]. In the past, the conjugate gradient (CG) and the biconjugate gradient (BCG) methods have been employed as such an iterative solver, and the resultant methods are often referred to as the CG–FFT and BCG–FFT methods [5]–[7]. The use of the so-called CG–FFT or BCG–FFT method reduces the memory requirement to $O(N)$ and computational complexity to $O(N_{\rm iter}N\log N)$, where $N_{\rm iter}$ denotes the number of CG or BCG iterations.

There is a large body of literature on the CG–FFT and BCG–FFT methods for a variety of electromagnetics problems and it is not our intention to review it here. Instead, we shall focus on those for 3-D volumetric material problems. The first application of the CG–FFT method to such problems can be found in the analysis of the absorption of electromagnetic power by human bodies [5]. However, the use of pulse basis functions yielded slow convergence and poor results when dealing with materials with high dielectric contrast. Better formulations were later proposed [8]–[14], and most used mixed-order (linear in one direction and constant in the other two directions) basis functions. Among these, the methods proposed by Zwamborn and van den Berg [10]–[12] and Gan and Chew [13] are the most accurate for materials with high dielectric contrast. In both methods, one is required to calculate (within each iteration) the multiplication between the transpose of the system matrix and a vector, in addition to that between the system matrix and a vector, resulting in at least 12 FFT's (including inverse FFT's) per iteration.

In this paper, we present an alternative and more efficient method for computing electromagnetic fields in arbitrarily shaped inhomogeneous dielectric bodies. In this method, a transpose-free quasi-minimal residual (TFQMR) algorithm [15] is employed to avoid the multiplication between the transpose of the system matrix and a vector, resulting in a much simpler computer implementation. Moreover, the number of FFT's is reduced to only six per iteration. It is observed that the TFQMR-FFT method yields excellent results even for highly inhomogeneous dielectric objects.

II. Formulation

Consider the problem of scattering by a lossy inhomogeneous dielectric object with a complex permittivity

$$\epsilon(\mathbf{x})=\epsilon_r(\mathbf{x})\epsilon_0-j\frac{\sigma(\mathbf{x})}{\omega} \tag{1}$$

where ϵ_r denotes the relative permittivity and σ denotes the electric conductivity of the object, which is in a free space having a permittivity ϵ_0. The incident electric field is denoted as $\mathbf{E}^{\rm inc}=(E_1^{\rm inc},\,E_2^{\rm inc},\,E_3^{\rm inc})^T$. The scattering problem can be formulated as the following domain integral equation over the object domain $\mathbf{V}$:

$$\frac{\mathbf{D}(\mathbf{x})}{\epsilon(\mathbf{x})}-(k_0^2+\nabla\nabla\cdot)\mathbf{A}(\mathbf{x})=\mathbf{E}^{\rm inc}(\mathbf{x}),\ \mathbf{x}\in\mathbf{V} \tag{2}$$

where $k_0=\omega\sqrt{\epsilon_0\mu_0}$ and

$$\mathbf{A}(\mathbf{x})=\frac{1}{\epsilon_0}\int_{\mathbf{V}}G(\mathbf{x}-\mathbf{x}')\chi(\mathbf{x}')\mathbf{D}(\mathbf{x}')d\mathbf{x}' \tag{3}$$

with

$$\chi(\mathbf{x})=\frac{\epsilon(\mathbf{x})-\epsilon_0}{\epsilon(\mathbf{x})}\quad G(\mathbf{x}-\mathbf{x}')=\frac{\exp(-jk_0|\mathbf{x}-\mathbf{x}'|)}{4\pi|\mathbf{x}-\mathbf{x}'|}.$$

To discretize this equation, we place the object in a uniform mesh with grid widths of Δx_1, Δx_2, and Δx_3 in the x_1-, x_2-, and x_3-directions, respectively. Therefore, the object is modeled approximately as a collection of small grids. The center of each grid is denoted as $\mathbf{x}_{M,N,P}=\left\{\left(M-\frac{1}{2}\right)\Delta x_1,\,\left(N-\frac{1}{2}\right)\Delta x_2,\,\left(P-\frac{1}{2}\right)\Delta x_3\right\}$ and within each grid the complex permittivity is assumed to be constant with value $\epsilon_{M,N,P}=\epsilon(\mathbf{x}_{M,N,P})$.

To convert (2) into a matrix equation, we expand the generalized electric flux density and the electric-contrast vector potential as

$$\mathbf{D}(\mathbf{x})=\epsilon_0\sum_{q=1}^{3}\sum_{I,J,K}d_{I,J,K}^{(q)}\mathbf{\Psi}_{I,J,K}^{(q)}(\mathbf{x}),\ \mathbf{x}\in\mathbf{V} \tag{4}$$

$$\mathbf{A}(\mathbf{x})=\sum_{q=1}^{3}\sum_{I,J,K}A_{I,J,K}^{(q)}\mathbf{\Psi}_{I,J,K}^{(q)}(\mathbf{x}),\ \mathbf{x}\in\mathbf{V} \tag{5}$$

where $\mathbf{\Psi}_{I,J,K}^{(1)}(\mathbf{x})$, $\mathbf{\Psi}_{I,J,K}^{(2)}(\mathbf{x})$, $\mathbf{\Psi}_{I,J,K}^{(3)}(\mathbf{x})$ are vector volumetric rooftop functions in x_1-, x_2-, and x_3-directions, respectively [10]–[13]. We then apply the Galerkin's testing formulation to (2) and obtain

$$\left\langle\mathbf{\Psi}_{M,N,P}^{(p)}(\mathbf{x}),\,\frac{\mathbf{D}(\mathbf{x})}{\epsilon(\mathbf{x})}\right\rangle-k_0^2\langle\mathbf{\Psi}_{M,N,P}^{(p)}(\mathbf{x}),\,\mathbf{A}(\mathbf{x})\rangle+\langle\nabla\cdot\mathbf{\Psi}_{M,N,P}^{(p)}(\mathbf{x}),\,\nabla\cdot\mathbf{A}(\mathbf{x})\rangle=\langle\mathbf{\Psi}_{M,N,P}^{(p)}(\mathbf{x}),\,\mathbf{E}^{\rm inc}(\mathbf{x})\rangle \tag{6}$$

for $p=1,\,2,\,3$, where $\langle\cdot\rangle$ denotes the inner product of two vector functions. Substituting (4) and (5) into (6), we obtain the following weak form of the domain integral equation:

$$[u_{M,N,P;I,J,K}^{(p,q)}][d_{I,J,K}^{(q)}]-[k_0^2v_{M,N,P;I,J,K}^{(p,q)}-w_{M,N,P;I,J,K}^{(p,q)}]\cdot[A_{I,J,K}^{(q)}]=[e_{M,N,P}^{{\rm inc},(p)}] \tag{7}$$

where

$$u_{M,N,P;I,J,K}^{(p,q)}=\langle\mathbf{\Psi}_{M,N,P}^{(p)},\,\frac{\epsilon_0}{\epsilon(\mathbf{x})}\mathbf{\Psi}_{I,J,K}^{(q)}\rangle$$

$$v_{M,N,P;I,J,K}^{(p,q)}=\langle\mathbf{\Psi}_{M,N,P}^{(p)},\,\mathbf{\Psi}_{I,J,K}^{(q)}\rangle$$

$$w_{M,N,P;I,J,K}^{(p,q)}=\langle\nabla\cdot\mathbf{\Psi}_{M,N,P}^{(p)},\,\nabla\cdot\mathbf{\Psi}_{I,J,K}^{(q)}\rangle$$

$$e_{M,N,P}^{{\rm inc},(p)}=\langle\mathbf{\Psi}_{M,N,P}^{(p)},\,\mathbf{E}^{\rm inc}\rangle.$$

The relationship between $d_{M,N,P}^{(q)}$ and $A_{M,N,P}^{(q)}$ can be found by substituting (4) and (5) into (3), yielding

$$A_{M,N,P}^{(q)}=\Delta V\sum_{I,J,K}G_{M-I,N-J,P-K}\chi_{I,J,K}^{(q)}d_{I,J,K}^{(q)}$$

or

$$[A_{M,N,P}^{(q)}]=\Delta V\,DFT^{-1}\{DFT[G_{M,N,P}]\cdot DFT[\chi_{M,N,P}^{(q)}d_{M,N,P}^{(q)}]\} \tag{8}$$

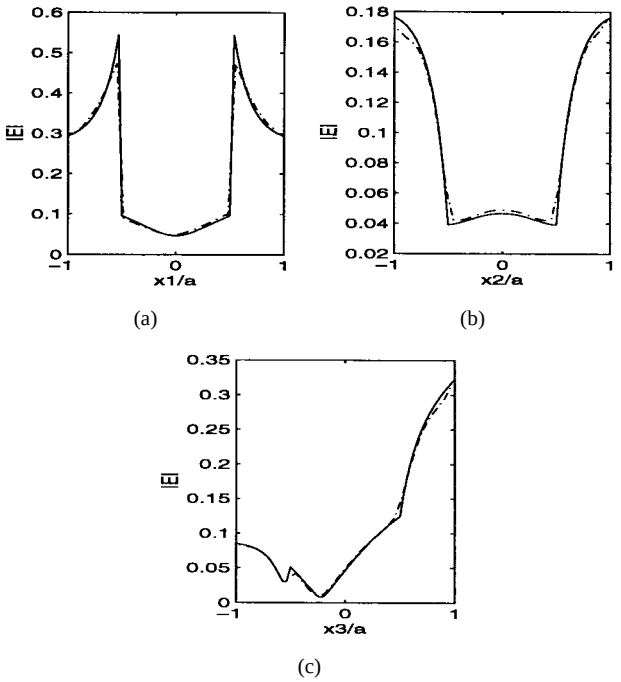

(a) (b) (c)

Fig. 1. Magnitude of the total electric field inside a two-layer dielectric sphere along the x_1-, x_2-, and x_3-axes. The inner layer has a radius $a_1 = 0.075$ m and $\epsilon_{1r} = 72.0 - j161.779$, and the outer layer has a radius $a_2 = 0.15$ m and $\epsilon_{2r} = 7.5 - j8.9877$, and the frequency is 100 MHz. The solid line is from the Mie series solution and the dash–dot line is from the TFQMR–FFT solution with grids $31 \times 31 \times 31$.

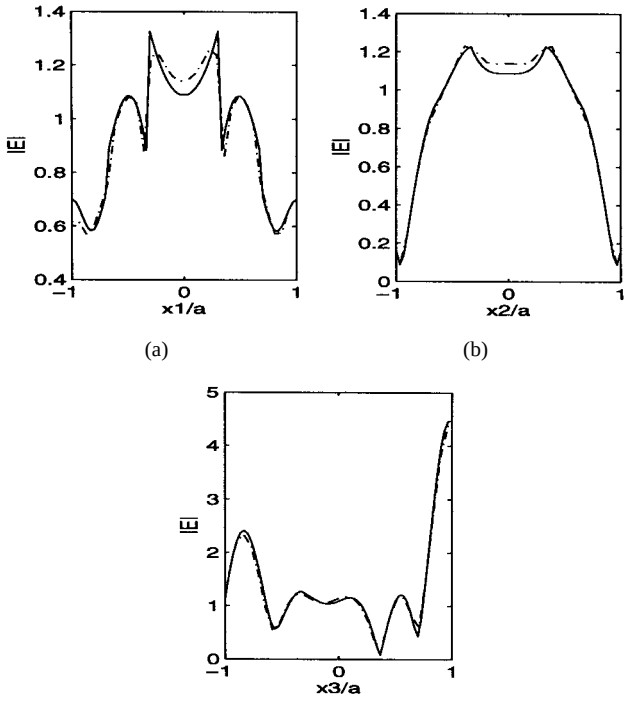

(a) (b) (c)

Fig. 2. The magnitude of the total electric field inside a three-layer dielectric sphere along the x_1-, x_2-, and x_3-axes. The inner layer has a radius $a_1 = 0.3333\lambda_0$ and $\epsilon_{1r} = 1.2$, the middle layer has a radius $a_2 = 0.6667\lambda_0$ and $\epsilon_{2r} = 2.0$, and the outer layer has a radius $a_3 = \lambda_0$ and $\epsilon_{3r} = 2.4$. The solid line is from the Mie series solution and the dash–dot line is from the TFQMR-FFT solution with grids $31 \times 31 \times 31$.

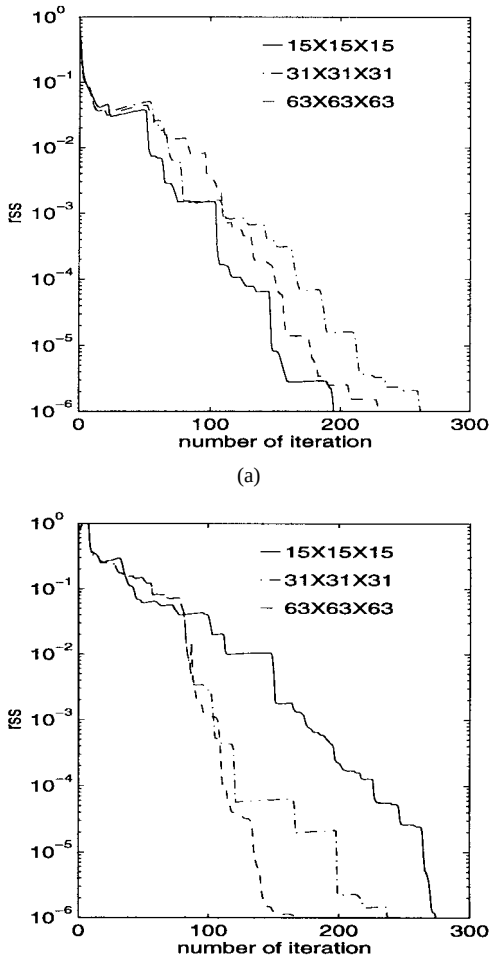

(a) (b)

Fig. 3. The relative error versus the number of iterations for different grid sizes. (a) For the case of the two-layer sphere. (b) For the case of the three-layer sphere.

TABLE I
COMPUTATION TIME AND STORAGE ON DEC ALPHA

Mesh size	FFT size	Number of unknowns	CPU-time per iteration	Computer storage
$15 \times 15 \times 15$	$32 \times 32 \times 32$	10800	0.74 sec	2.2 Mb
$31 \times 31 \times 31$	$64 \times 64 \times 64$	92256	9.5 sec	16 Mb
$63 \times 63 \times 63$	$128 \times 128 \times 128$	762048	152 sec	105 Mb

where $\Delta V = \Delta x_1 \Delta x_2 \Delta x_3$. Substituting (8) into (7), we obtain a system of linear algebraic equations, which can be symbolically written as

$$\mathbf{L}\mathbf{d} = \mathbf{e}^{\mathrm{inc}}. \tag{9}$$

The formulation described above was first proposed by Zwamborn and van den Berg [10]–[12]. Its major advantage is the simplicity in treating the singularity of the integrals in (2) and, more important, in calculating the right-hand side of (7), which is accomplished through two stages. The first stage is to calculate $A^{(q)}_{M,N,P}$ from (8) and the second stage is to substitute it into (7). Note that the matrices implied in (7) are sparse matrices and their product with a vector can be evaluated with $O(N_T)$ operations, where N_T denotes the number of unknowns. Although the matrix implied in (8) is a dense matrix,

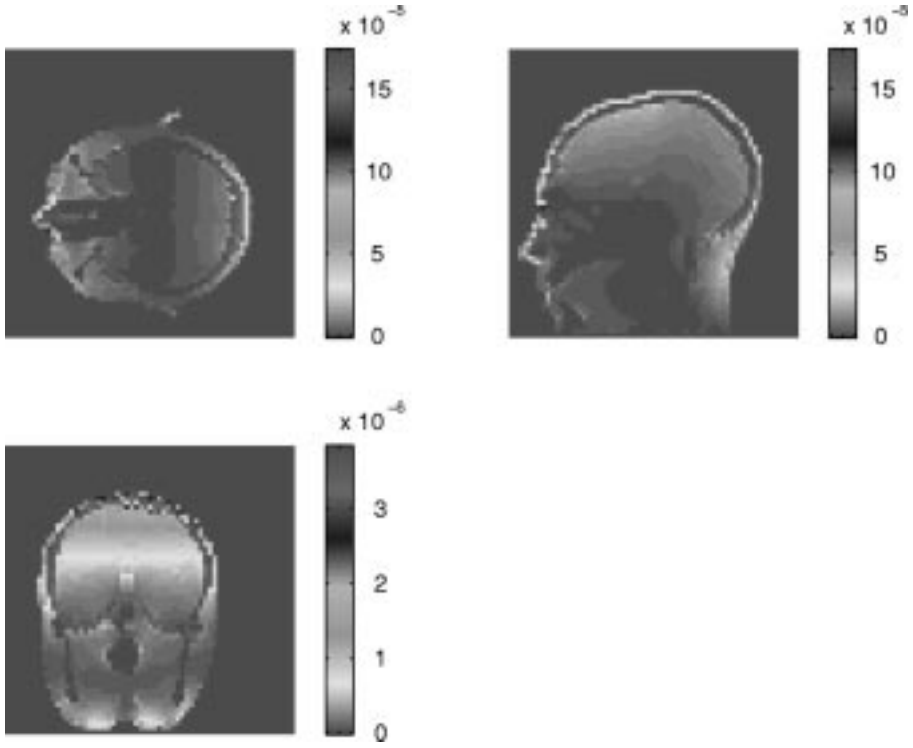

Fig. 4. SAR (watt/kilogram) in the axial, sagittal, and coronal slices at 64 MHz for a uniform plane-wave excitation polarized in the x_1-direction and propagating in the $-x_3$-direction using 63 $\times$ 63 $\times$ 63 grids.

the computation of its product with a vector can be evaluated with $O(N_T \log N_T)$ operations with the aid of the FFT.

III. TFQMR–FFT Iterative Algorithm

Once (9) is formulated, its solution yields a numerical solution to the original problem. However, since the number of unknowns in (9) is usually very large, its solution, using a direct solver such as Gaussian elimination and LU decomposition method, is basically impractical because a direct solver has a memory requirement of $O(N_T^2)$ and computational complexity of $O(N_T^3)$. This difficulty can be circumvented by solving (9) by using an iterative solver, and in each iteration the required matrix-by-vector product is evaluated using the FFT, as pointed out earlier. In the past, the CG and BCG methods have been employed as such an iterative solver, and the resultant methods are referred to as the CG–FFT and BCG–FFT methods [5]–[14]. The use of these methods reduces the memory requirement to $O(N_T)$ and computational complexity to $O(N_{\rm iter} N_T \log N_T)$, where $N_{\rm iter}$ denotes the number of CG or BCG iterations. However, both CG–FFT and BCG–FFT algorithms require the calculation of a matrix-by-vector product with the conjugate transpose of the system matrix, which in most cases is not an easy task since the system matrix in (9) is nonsymmetric. Furthermore, the CG method has a problem of slow convergence, although it converges monotonically, and the BCG method does not guarantee convergence, although it usually converges quickly. Although this problem can be alleviated by using the QMR method [16], which converges monotonically with a convergence rate similar to the BCG method, the QMR still requires the calculation of a matrix-by-vector product with the conjugate transpose of the system matrix. Here, we consider other alternatives.

There are four algorithms that do not require the calculation of the transpose of the system matrix. The first one is the CG-squared (CGS) algorithm [17], which is the transpose-free variant of the BCG algorithm. However, like the BCG method, it also exhibits a rather irregular convergence behavior with wild oscillations in residual norm and does not guarantee convergence. The second method is the BCG stabilized (BCGSTAB) algorithm [18], which uses local steepest descent steps to obtain a more smoothly convergent process. While this algorithm seems to work well in many cases, it still exhibits the irregular convergence behavior for some difficult problems. Also, its convergence is considerably slower than the CGS algorithm. The third method is the transpose-free QMR (TFQMR) method [15]. This algorithm can be implemented easily by changing only a few lines in the standard CGS algorithm. However, unlike the CGS algorithm, the iterations of the TFQMR algorithm are characterized by a quasi-minimization of the residual norm. This leads to smooth convergence with a convergence rate similar to the CGS algorithm. The TFQMR algorithm can be considered as a new version of the CGS algorithm which "quasi-minimizes" the residual in the space spanned by the vectors generated by the CGS iterations. Recently, a QMR variant of the BCGSTAB algorithm (QMRBCGSTAB) [19] is proposed. Our experimental calculation shows, however, that its convergence can be slower than the TFQMR for our problems. After a comprehensive comparison, the TFQMR algorithm is chosen for this paper.

The TFQMR algorithm for solving (9) can be found in [15] and [20]. From the algorithm, it is observed that each odd iteration requires two matrix-by-vector products and each even iteration does not require a matrix-by-vector product. Therefore, on average, the TFQMR algorithm requires only one matrix-by-vector product, which can be calculated using six FFT's.

IV. Numerical Results

To demonstrate the accuracy of the TFQMR-FFT algorithm, we analyze the scattering of a plane wave from two layered dielectric spheres and compare the results with the Mie series solution. In all simulations, we assume that the incident plane wave is polarized in the x_1-direction and propagates in the x_3-direction and the background is the free space. The amplitude of the incident electric field is 1 V/m. The first sphere has two layers and the second sphere

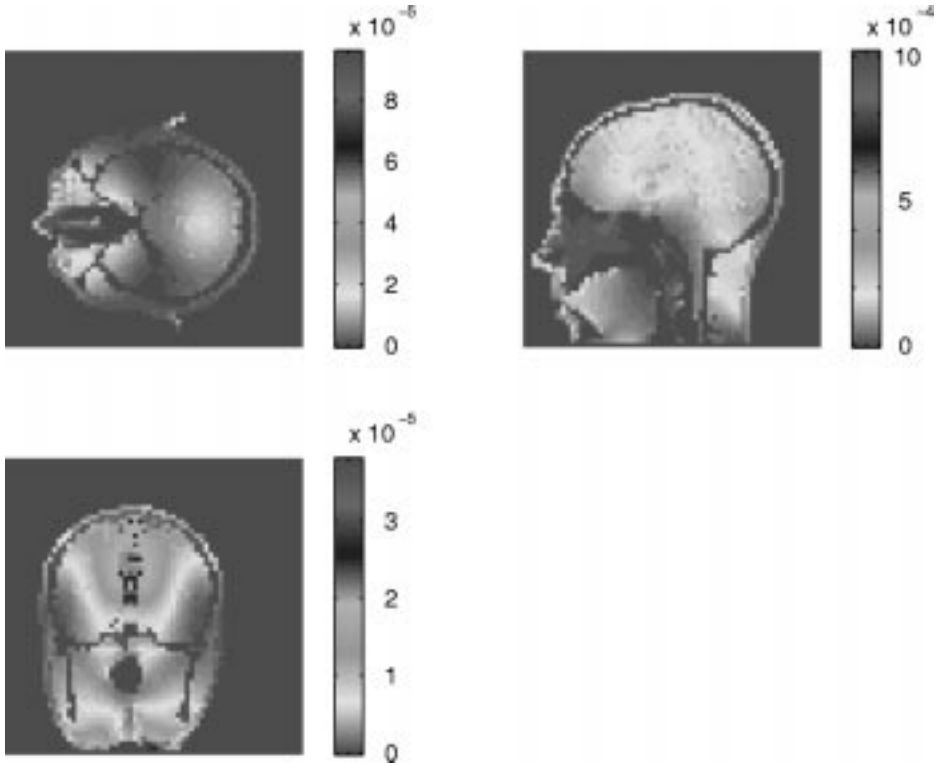

Fig. 5. SAR (watt/kilogram) in the axial, sagittal, and coronal slices at 256 MHz for a uniform plane wave excitation polarized in the x_1-direction and propagating in the $-x_3$-direction using 63 $\times$ 63 $\times$ 63 grids.

has three layers. Fig. 1 shows the field in the two-layer dielectric sphere, and Fig. 2 gives the results for the three-layer sphere. The convergence criterion for these results is $rss = \|\mathbf{r}_m\|/\|\mathbf{r}_0\| < 10^{-3}$. Excellent agreement is observed between the exact solution and the numerical results obtained using 31 $\times$ 31 $\times$ 31 grids. The relative error versus the number of iterations is given in Fig. 3 for both cases for different grid sizes. As can be seen, the TFQMR–FFT algorithm exhibits a stable convergence behavior. The computation time needed to evaluate one iteration, the total number of unknowns, and the required computer storage are given in Table I.

To demonstrate the efficiency of the algorithm, we consider again the problem illustrated in Fig. 1. As can be seen in Fig. 3(a), using the TFQMR–FFT algorithm with 31 $\times$ 31 $\times$ 31 grids, it takes 112 iterations to reduce rss below 10^{-3}. Since each iteration requires six FFT's, the total number of FFT's is 672. This problem was also treated using the CG–FFT algorithm in [10]–[12] and the BCG-FFT algorithm in [13]. For the same grid size and accuracy, the CG–FFT algorithm takes about 360 iterations and, since each iteration requires 12 FFT's, the total number of FFT's is about 4320, which is 6.4 times that of the TFQMR–FFT algorithm. When the BCG–FFT algorithm is used, it takes only 54 iterations and, since each iteration requires 18 FFT's, the total number of FFT's is 972, which is 1.4 times that of the TFQMR–FFT algorithm. Furthermore, the BCG-FFT algorithm has an irregular convergence behavior and does not guarantee convergence.

Finally, to demonstrate the capability of the TFQMR–FFT algorithm to treat a strongly inhomogeneous dielectric object, we consider the plane wave scattering by a human head. The construction of the electromagnetic model of the head is discussed in [21] and the material property of the tissues of the head is given in [22]. The incident wave propagates in the $-x_3$-direction (from top) and the incident electric field is polarized in the x_1-direction (from the left-to-right ear). The incident electric field has an amplitude of 1 V/m

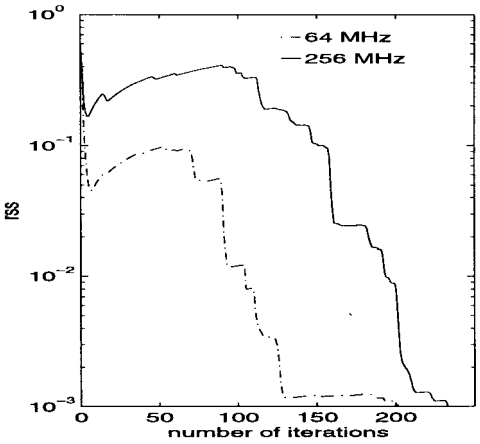

Fig. 6. The relative error versus the number of iterations for different frequencies with 63 $\times$ 63 $\times$ 63 grids. (a) For the case of 64 MHz. (b) For the case of 256 MHz.

and the frequencies considered are 64 and 256 MHz. The results are presented in the form of spatial absorption rate (SAR) defined as SAR $= \sigma|\mathbf{E}|^2/2\rho$, where ρ denotes the density. Figs. 4 and 5 show the SAR in the axial, sagittal, and coronal planes at the two frequencies. Fig. 6 shows the relative error versus the number of iterations for the two frequencies. Again, the TFQMR–FFT algorithm exhibits a stable convergence behavior.

V. Conclusion

This paper has presented a TFQMR–FFT algorithm for computing electromagnetic fields in a 3-D arbitrarily shaped inhomogeneous dielectric body. It is observed that this algorithm yields excellent results and exhibits a very stable convergence behavior. Because of

the use of the TFQMR method, the algorithm avoids the computation of the multiplication between the transpose of the system matrix and a vector, which is required in both the CG–FFT and BCG–FFT methods. As a result, the programming complexity is greatly reduced. Furthermore, since on average the TFQMR method requires only one matrix-by-vector multiplication, which can be evaluated using six FFT's, the TFQMR–FFT algorithm is more efficient than the currently available CG–FFT and BCG–FFT methods.

REFERENCES

[1] D. E. Livesay and K. M. Chen, "Electromagnetic fields induced inside arbitrarily shaped biological bodies," *IEEE Trans. Microwave Theory Tech.*, vol. MTT-22, pp. 1273–1280, Dec. 1974.

[2] D. H. Schaubert, D. R. Wilton, and A. W. Glisson, "A tetrahedral modeling method for electromagnetic scattering by arbitrarily shaped inhomogeneous dielectric bodies," *IEEE Trans. Antennas Propagat.*, vol. AP-32, pp. 77–85, Jan. 1984.

[3] R. D. Graglia, P. L. E. Uslenghi and R. S. Zich, "Moment method with isoparametric elements for three-dimentional anisotropic scatters," *Proc. IEEE*, vol. 5, pp. 750–760, July 1989.

[4] N. N. Bojarski, "$\bar{K}$-Space formulation of the electromagnetic scattering problems," Air Force Avionic Lab. Tech. Rep. AFAL-TR-71-75, 1971.

[5] D. T. Borup and O. P. Gandhi, "Fast-Fourier transform method for calculation of SAR distributions in finely discretized inhomogeneuos models of biological bodies," *IEEE Trans. Microwave Theory Tech.*, vol. MTT-32, pp. 355–360, Apr. 1984.

[6] T. K. Sarkar, E. Arvas, and S. M. Rao, "Application of FFT and the conjugate gradient method for the solution of electromagnetic radiation from electrically large and small conducting bodies," *IEEE Trans. Antennas Propagat.*, vol. AP-34, pp. 635–640, May 1986.

[7] J. M. Jin and J. L. Volakis, "A biconjugate gradient FFT solution for scattering by planar plates," *Electromagnetics*, vol. 12, no. 1, pp. 105–119, 1992.

[8] M. F. Catedra, E. Gago, and L. Nuno, "A numerical scheme to obtain the RCS of three-dimensional bodies of size using the conjugate gradient method and the fast Fourier transform," *IEEE Trans. Antennas Propagat.*, vol. 37, pp. 528–537, Apr. 1989.

[9] C. Y. Shen, K. J. Glover, M. I. Sancer, and A. D. Varvatsis, "The discrete Fourier transform method of solving differential-integral equations in scattering theory," *IEEE Trans. Antennas Propagat.*, vol. 37, pp. 1032–1041, June 1989.

[10] P. Zwamborn and P. M. van der Berg, "The three-dimensional weak form of the conjugate gradient FFT method for solving scattering problems," *IEEE Trans. Microwave Theory Tech.*, vol. 40, pp. 1757–1766, Sept. 1992.

[11] A. P. M. Zwamborn, P. M. van der Berg, J. Mooibroek, and F. T. C. Koenis, "Computation of three-dimensional electromagnetic-fields distributions in a human body using the weak form of the CGFFT method," *ACES J.*, vol. 7, pp. 26–42, 1992.

[12] A. P. M. Zwamborn and P. M. van der Berg, "Computation of electromagnetic fields inside strongly inhomogeneous objects by the weak-conjugate-gradient fast-Fourier-transform method," *J. Opt. Soc. Amer. A, Opt. Image Sci.*, vol. 11, pp. 1414–1420, 1994.

[13] H. Gan and W. C. Chew, "A discrete BCG-FFT algorithm for solving 3D inhomogeneous scattering problems," *J. Electromagn. Wave Applicat.*, vol. 9 , no. 10, pp. 1339–1357, 1995.

[14] J. H. Lin and W. C. Chew, "BiCG-FFT T-matrix method for the scattering solution from inhomogeneous bodies," *IEEE Trans. Microwave Theory Tech.*, vol. 44, pp. 1150–1155, July 1996.

[15] R. W. Freund, "A transpose-free quasiminimal residual algorithm for non-Hermitian linear systems," *SIAM J. Sci. Stat. Comput.*, vol. 14, no. 2, pp. 470–482, 1993.

[16] R. W. Freund and N. M. Nachtigal, "A quasiminimal residual method for non-Hermitain linear systems," *Numer. Math.*, vol. 60, pp. 315–339, 1991.

[17] P. Sonneveld, "CGS, a fast Lanczos-type solver for nonsymmetric linear systems," *SIAM J. Sci. Stat.. Comput.*, vol. 10, pp. 36–52, 1989.

[18] H. A. van Der Vorst, "BI-CGSTAB: A fast and smoothly converging variant of BI-CG for the solution of nonsymmetric linear systems," *SIAM J. Sci. Stat. Comput.*, vol. 13, pp. 631–644, 1992.

[19] T. F. Chan, E. Gallopoulos, V. Simoncini, T. Szeto, and C. H. Tong, "A quasiminimal residual variant of the BI-CGSTAB algorithm for nonsymmetric systems," *SIAM J. Sci. Stat. Comput.*, vol. 15, no. 2, pp. 338–347, 1994.

[20] Y. Saad, *Iterative Method for Sparse Linear Systems*. New York: PWS, 1995.

[21] P. J. Dimbylow and S. M. Mann, "SAR calculations in an anatomically realistic model of the head for mobile communication transceivers at 900 MHz and 1.8 GHZ," *Phys. Med. Biol.*, vol. 39, pp. 361–368, 1994.

[22] J. M. Jin, J. Chen, H. Gan, W. C. Chew, R. L. Magin, and P. J. Dimbylow, "Computation of electromagnetic fields for high-frequency magnetic resonance imaging applications," *Phys. Med. Biol.*, vol. 41, pp. 2719–2738, 1996.

Two-Dimensional Wavelet-Analysis of a Microstrip Open

Gerald Oberschmidt, Karsten Bubke, and Arne F. Jacob

***Abstract*— Simple two-dimensional (2-D) wavelet systems are used in a moment method to analyze a microstrip discontinuity. This allows one to efficiently compress the impedance matrix. The achievable sparsity is discussed for different resolution depths where up to 85% was obtained for an error below 1%.**

***Index Terms*— Matrix compression, numerical analysis, planar microwave circuits, wavelets.**

I. INTRODUCTION

The spectral-domain moment method is known to be a very effective tool for the analysis of planar microwave circuits [1]. It leads, however, to densely populated impedance matrices. For large or complex circuit configurations, this can become a serious problem because of limited computer resources. This drawback can be overcome by discretizing with wavelet bases because they allow compression of the impedance matrices [2]–[5].

Wavelet bases have recently been used to effectively analyze two-dimensional (2-D) structures [3]. Here, the wavelet scheme has been extended to two dimensions, similar to [6].

After briefly reviewing the method and the concept of wavelets, we present the construction of tensor wavelets in two dimensions with arbitrary resolution levels in both directions. Details about the implementation of the program are followed by a discussion of the results.

II. METHOD

To analyze an open microstrip line, the electric-field integral equation (EFIE) is solved in the spectral domain [1]. Since for electrically narrow strips the transverse current can be neglected [3], the EFIE reduces to

$$\tilde{E}_x(\alpha, \beta, h) = \tilde{G}_{xx}(\alpha, \beta)\tilde{J}_x(\alpha, \beta, h) \tag{1}$$

for the longitudinal components of the electric field and current density. Here, α and β are the x- and y-space frequencies, respectively, and h is the height of the substrate. The tilde denotes the Fourier transform. Definitions and notations, especially for the Green's function $\tilde{G}_{xx}$, are as in [1].

Manuscript received September 30, 1996; revised February 14, 1998.

The authors are with the Institut für Hochfrequenztechnik, Technische Universität Braunschweig, 38023 Braunschweig, Germany (e-mail: G.Oberschmidt@tu-bs.de; A.Jacob@tu-bs.de).

Publisher Item Identifier S 0018-9480(98)03170-6.